Bulletin of Geophysics and Oceanography Vol. 62, n. 4, pp. 615-636; December 2021
DOI 10.4430/bgta0354

Relationships between reservoir permeability, magmatism and the development of geothermal systems in continental settings

G. Gola

Institute of Geosciences and Earth Resources, National Research Council of Italy, Pisa, Italy

(Received: 20 November 2020; accepted: 8 February 2021; published online: 21 October 2021)

ABSTRACT A two-dimensional, time-dependent, numerical study of natural convection in porous media is presented. The finite element models are based on an idealised crustal section, including the main structural features characterising many hydrothermal systems. The onset of the thermal convection is investigated by exploring different thermal boundary conditions, accounting for variable permeability values of the geothermal reservoir and the presence of middle-crustal magmatic intrusions (10 km deep) as well as upper-crustal plutons (5 km deep). The basic mathematical framework for convection in porous media governed by Darcy's Law is outlined together with an ensemble of constitutive laws useful in the description of the macroscopic behaviour of the magmatic heat source and the porous rocks. The results are analysed together with the key parameter for convection, the Rayleigh number. Large-scale convective cells develop at moderate-to-high Rayleigh numbers, when the reservoir permeability overcomes a threshold value of the order 10^{-15}-10^{-14} m^2. The temporal evolution of the surface heat flow above the hydrothermal system, together with the 2D thermal structure around the magmatic heat source and within the geothermal reservoir, are also investigated and discussed.

Key words: hydrothermal systems, magmatic environment, geothermal energy, numerical simulations.

1. Introduction

Heat transfer occurs by three different mechanisms: conduction, advection, and radiation. The thermal conduction, i.e. the transfer of internal energy by microscopic collisions of particles within a solid, is the leading heat transport process in the Earth's lithosphere (Clauser, 2009). When rock temperature exceeds several hundred Celsius degrees, the thermal radiation, i.e. the electromagnetic radiation generated by the thermal motion of particles in solid, begins to sizably contribute to the overall heat transfer in most polycrystalline materials and its contribution cannot be neglected in thermal studies involving the upper mantle (Gibert *et al*., 2003, 2005). The heat advection by free or forced convection shows an important role in near-surface regions with high crustal permeability. As circulating fluids carry out a not negligible amount of thermal energy, groundwater flow influences the distribution of the temperature field in the Earth's crust (Ingebritsen *et al.*, 2006; Kooi, 2016).

The thermal structure of the Earth's lithosphere is typically predicted on the basis of the terrestrial heat flow observations and inferences on the layered thermal conductivity and radiogenic heat production distributions (Chapman *et al*., 1984; Stein, 1995; Majorowicz *et al*., 2019; Verdoya

et al., 2019). A broadly used approach assumes a horizontally layered, isotropic Earth governed by a steady-state, conductive thermal regime (Funnel *et al.*, 1996; Verdoya *et al*., 2021). These assumptions are valid in stable continental areas, which are mostly in, or close to, thermal steady-state (Jaupard *et al*., 2015). Deviations from these conditions may result both from deep tectono-thermal signals and hydrothermal circulation (Ranalli and Rybach, 2005; Cloetingh *et al*., 2010).

The onset of free convection depends on various factors, such as rock permeability, temperature gradient, thickness of the permeable layer and fluid properties. Locally, borehole temperature profiles show various signs of subsurface fluid movement, such as shallow high geothermal gradients, isothermal sections or even temperature reversals (Castaldo *et al*., 2017; Montanari *et al*., 2017). In these circumstances the assumption of a purely-conductive, steady-state thermal regime fails. In tectono-magmatic environments, the emplacement of a deep-seated magmatic body results in a large thermal perturbation, which is dispersed by both heat diffusion (conduction) and fluid circulation (convection). The generation of a fluid potential field is a direct consequence of a thermally-driven density instability within the water column (free convection), superimposed on a background fluid flow driven by the natural recharge and topographic irregularities (forced convection).

Although the upward migration of deep fluids from the lower crust assumes a crucial role in the regional metamorphism (Harlov, 2012), at middle-to-lower crustal levels (z > 10-15 km) the permeability of the metamorphic rocks limits a significant convective heat transport operated by the deep crustal fluids, so that the resulting temperature distribution is mainly controlled by thermal conduction (Manning and Ingebritsen, 1999; Ingebritsen and Manning, 2003). Conversely, in upper crustal layers (z < 5-10 km), higher permeability values allow a more efficient convective heat transport, especially in sedimentary basins. However, also in crystalline rocks, where primary porosity is negligible, the capability to channel fluids is guaranteed by open fracture networks (Stober and Bucher, 2014). In this context, extensional normal faults and brittle shear zones, which may affect the crust down to the brittle/ductile transition, play a key role in controlling the fluid paths at large depths, as recognised both in exhumed geothermal systems (Liotta *et al*., 2015) and active geothermal areas (Brogi *et al*., 2005) in the Tuscan Archipelago and the inner zone of the northern Apennines, respectively. In active magmatic areas, an additional aspect consists in the rheological control of the host rocks (e.g. strengths and temperature of the continental crust) on the magma ascent and its emplacement within the crust (Gorczyk and Vogt, 2018). The initial yield strength of the crust controls the different modes of intrusion (e.g. dikes, cone sheets, sills, plutons), the surface uplift as well as the degree of crustal faulting. In turn, these fractures are potential pathways for magma-derived fluids.

From a conceptual point of view, a hydrothermal system is characterised by five specific features (Santilano *et al*., 2015; DiPippo, 2016): i) a heat source, such as a cooling crustal magma body or a high regional heat flow due to tectonic processes, allowing the rock formation to reach elevated temperatures; ii) a permeable volume of rock, corresponding to the geothermal reservoir hosted in geological units having interconnected porosity and/or open fracture networks; iii) the presence of a heat transfer fluid, which enhances the energy transport in the permeable formation; iv) the occurrence of a natural recharge, such as rainfall or snow melt, which supplies water to the reservoir; and v) an impermeable cap-rock, which seals the deep-seated reservoir from the surface, preventing heat and mass dispersion. Where the above-mentioned favourable geological conditions lead to the development of a deep-seated hydrothermal system, the thermal energy transported by the upwelling fluids is responsible for surface heat flow values that, in young magmatic areas, are well beyond 10^2 mW·m^{-2} and, locally, can even reach 10^3

$mW \cdot m^{-2}$ (Bellani *et al*., 2004). In this circumstance, the convective component of the observed heat flow results larger than the conductive one (Norton, 1977; Norton and Knight, 1977).

Thanks to the availability of high-temperature geothermal fluids, the young magmatic geological provinces represent the most interesting areas where geothermal exploration focus. For this reason, the knowledge of the age of the last magmatic event, as well as the emplacement depth and temperature of the magmatic intrusion, are essential aspects allowing us to characterise the hydrothermal system and assessing its geothermal potential (Gola *et al*., 2017, 2021). Moreover, how long magma bodies persist in the middle-to-upper crust is a fundamental information to unravel the relationship between magmatism and the development of hydrothermal systems in continental settings.

In this work, the evolution of the temperature distribution in a layered crust accounting for the presence of a magmatic heat source has been investigated both in conductive and convective thermal regimes. Albeit with some simplifications, the numerical models describe the thermal evolution around a magmatic intrusion taking into account the relevant physical processes. A sequence of numerical experiments is resolved in order to ascertain the effects of a number of geological parameters on heat and fluid transport phenomena. Among all the possible variables, the time-dependent temperature distribution is explored by varying the pluton size, its emplacement depth, as well as the rock permeability of the overlying geothermal reservoir.

2. Methods

The most important feature of the high-temperature hydrothermal systems is the effectiveness of the heat source represented by crustal magmatic intrusions. The geological mechanisms leading to melting of the lithosphere, magma segregation and its migration in the Earth's crust are key issues. A comprehensive overview of granitic magma generation, ascent and emplacement can be found in Petford *et al*. (2000) and Annen *et al*. (2008). Given the average thickness of the continental lithosphere (~100 km), a typical conductive geotherm constrained by a mantle potential temperature of 1300 °C (Wang and Currie, 2015; Shellnutt and Thuy, 2018) does not generate temperatures high enough to melt common crustal rocks, although volumes of mafic melts can be produced at large depths by hydration processes of the mantle lithosphere (Liu *et al*., 2017). In order to attain melting temperatures at shallower depths, the thinning of the lithosphere resulting from extensional tectonic and lithospheric erosion has been invoked as the driving mechanism to explain regional high thermal anomalies and associated magmatic processes in either off-shore or continental areas, like in the Tyrrhenian basin and the inner sector of the northern Apennines (Pasquale *et al*., 2010). In Fig. 1A, the above-mentioned conceptual models for melting under continents are displayed.

The numerical procedure presented here simulates the time-dependent temperature and fluid pressure variations in a layered crust induced by a fast emplacement and successive cooling of a hot magmatic body over a time interval of 1.0 Myr. The simulated time interval does not represent a specific geological period but allows the simulations to reach a quasi-steady-state solution. Based on analytically obtained magma ascent velocities in highly porous rocks as high as 10-1000 m/yr (Turner and Costa, 2007), an instantaneous magmatic emplacement is a reasonable assumption. Tough the effects of an incremental growth of the magmatic chamber (or pluton) are neglected, the magmatic emplacement temperature is kept constant for a given time interval accounting for a likely rate of replenishment from below (see section 2.2).

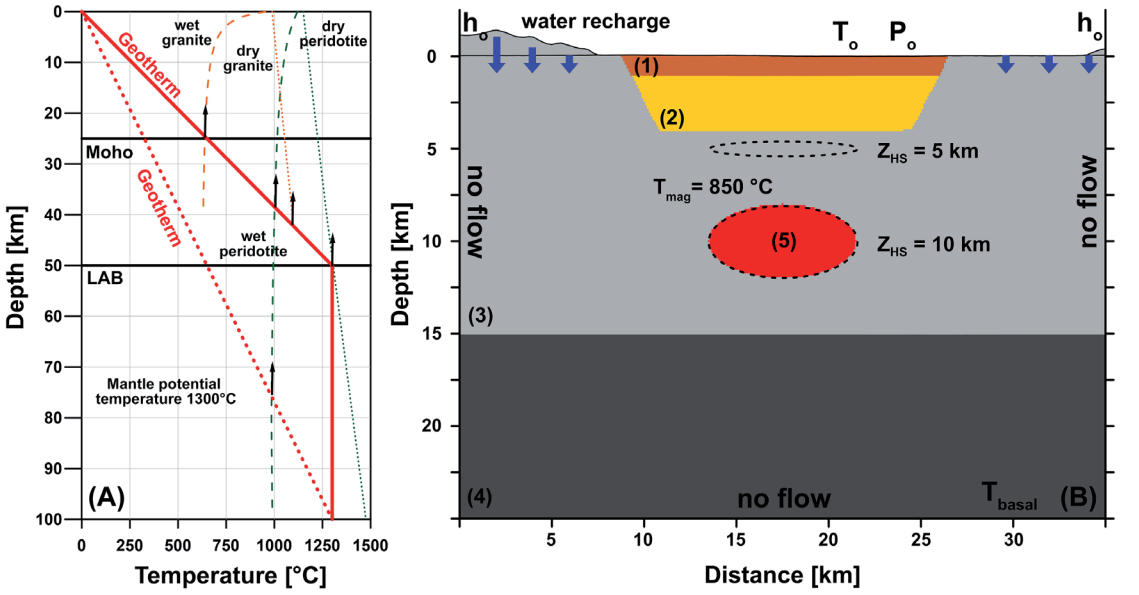

Fig. 1 - Thermal model: A) conceptual models for melting under continents: the approximate wet (dashed) and dry (dotted) solidi are shown for both granite (a proxy for the felsic crust, in orange) and peridotite (a proxy for both lower lithosphere and mantle, in green). The melting temperatures are computed as function of pressure by applying the equations in Gorczyk and Vogt (2018) and assuming a density of 2900 kg·m^{-3}, 3000 kg·m^{-3}, and 3300 kg·m^{-3} for the felsic crust, mafic crust, and mantle, respectively. With a mantle potential temperature of 1300 °C, the cold geotherm (dotted line) displays the difficulty of producing mantle melt under thick lithosphere (lithosphere-asthenosphere boundary-LAB at 100 km). When the lithosphere is thinned by half (LAB at 50 km), in upper mantle and lower crust, ambient temperatures exceed the wet solidi and are very close to the dry solidi, creating the conditions for melting. The black arrows show the depth to intersection of the linear lithospheric thermal gradient with the dry and wet solidi; B) geometry setting of the 2D numerical models: the lithothermal units used as input to build the models are: 1) the cap-rock, 2) the reservoir, 3) the upper crust, 4) the lower crust, and 5) the magmatic heat source. The dashed ellipsoids represent the magmatic heat sources set at different emplacement depths (Z_{HS} = 10 km and 5 km b.s.l.). The boundary conditions of the conductive-convective problem (T_o: surface temperature; P_o: surface pressure; h_o: hydraulic head; T_{basal}: basal temperature, T_{mag}: magmatic temperature) are displayed. Blue arrows highlight the water recharge zones.

In presence of a heat source, the fluid circulation is controlled by: i) external forces, i.e. the regional hydraulic gradients determined by the variations in the topographic elevation of the recharge areas, and ii) internal forces, i.e. the buoyancy forces within the water column triggered by thermally-driven density differences. As fluid flow in fractured rocks differs from porous media flow, for practical purposes, the numerical models assume that a representative elementary volume exists over which fracture permeability can be described by an equivalent porous medium approximation (Ingebritsen *et al.*, 2010). Other important assumptions are that a single-phase fluid (H_2O) circulates in the subsurface and it does not react with the hosting rocks. Although in real hydrothermal reservoirs of magmatic origin, geochemical evidence suggests that reactive and multi-component fluid flow occur (Chiodini *et al.*, 2003, 2004), here the numerical aspects covering precipitation and dissolution of minerals, commonly referred to as "reactive transport" are not accounted for. The assumption that pure water circulates in the subsurface allows an accurate description of the physical properties of the fluid (i.e. density, viscosity, thermal conductivity, and heat capacity) in the pressure-temperature domain according to IAPWS-IF97 (Wagner and Kretzschmar, 2008). As some level of approximation of fluid properties remains ubiquitous in hydrothermal modelling, the assumption that the normal

or expected circulating fluid in the upper continental crust is meteoric water is a widely accepted simplification, even in magmatic settings (e.g. Della Vedova *et al.,* 2008; Ingebritsen *et al*., 2010; Ebigbo *et al*., 2016; Montanari *et al*., 2017). Moreover, the single-phase simplification sensibly reduces the computational time allowing us to numerically investigate the sensitivity of the key parameters and boundary conditions (Castaldo *et al*., 2017). The different simulated scenarios are summarised in Table 1.

The governing partial differential equations (see section 2.2) are solved numerically through the finite element method by using the Comsol Multiphysics® software. A triangular mesh grid is defined, counting ~$16 \cdot 10^3$ elements with edge's dimension variable from 50 to 500 m. The temporal step-size Δt at which the solutions are written out is set to 500 yr. Nevertheless, it does not correspond to the time-step the numerical solver takes, which follows an adaptive time-stepping scheme. During the solution of the time-dependent problem, the solver may use internally smaller time-steps, if needed, to resolve any fast variations in the solution preserving a user-defined accuracy, here set to 10^{-3}. Therefore, smaller time-steps are used when solving for the temperature distribution during the fast magmatic emplacement event, as well as during the cooling of the magmatic body accounting for the latent heat of crystallisation.

Table 1 - Summary of the parameters used in the steady-state and time-dependent thermal models. Z_{HS} is the centroid depth of the magmatic heat source, H_{HS} is its maximum vertical extension, and $K_{o\,RES}$ is the superficial permeability of the reservoir unit.

Model		Z_{HS} (km)	H_{HS} (km)	$K_{o\,RES}$ (m^2)
1	steady-state	-	-	-
2a	time-dependent	10	4	-
2b		5	1	-
3a		-	-	$1 \cdot 10^{-15}$
3b		-	-	$1 \cdot 10^{-14}$
3c		-	-	$1 \cdot 10^{-13}$
4a		10	4	$1 \cdot 10^{-15}$
4b		10	4	$1 \cdot 10^{-14}$
4c		10	4	$1 \cdot 10^{-13}$
5a		5	1	$1 \cdot 10^{-15}$
5b		5	1	$1 \cdot 10^{-14}$
5c		5	1	$1 \cdot 10^{-13}$

2.1. Geometrical model

The two-dimensional thermal models are solved assuming a standard continental profile (Chapman, 1986), as depicted in Fig. 1B. The cross-section involves an approximately 26-km thick crust with a lateral extension of 35 km. At its top, an irregular topographic relief is accounted for, defining a background, regional fluid flow from the recharge zones. The crustal domains include

four main lithothermal units corresponding to, from the top to the bottom: i) the impervious cap-rock (unit 1, 1 km thick), ii) the permeable reservoir (unit 2, 3 km thick), iii) the crystalline basement (unit 3, ~16 km thick) matching the upper crustal layer supposed to be granodioritic in composition (Weaver and Tarney, 1984; Meissner, 1986; Brown and Mussett, 1993), and iv) the lower crust (unit 4, 10 km thick) of mafic composition (Schmid and Wood, 1976; Hunziker and Zingg, 1980; Sills, 1984; Pittarello *et al.*, 2012). The topology of the deep-seated magmatic body (unit 5) is defined by a simple ellipsoid, whose dimension and emplacement depth change in the different simulated scenarios. The geometrical models assume: i) a middle-crustal magmatic intrusion, with an emplacement depth (referred to the centre of the ellipsoid) of 10 km b.s.l. and a maximum vertical axis of 4 km; and ii) an upper-crustal pluton, with an emplacement depth of 5 km b.s.l. and a maximum vertical extension of 1 km. A common horizontal extension of 10 km is defined.

2.2. Thermal model

The heat and fluid transfer processes are described by the combination of the mass, momentum and energy conservation equations:

$$\rho_w \nabla \cdot \mathbf{u} = 0 \tag{1}$$

$$\mathbf{u} = -\frac{K_r}{\mu_w}(\nabla p + \rho_w \mathbf{g} \nabla z) \tag{2}$$

$$(\rho c_P)_r \frac{\partial T}{\partial t} = k_r \nabla^2 T - (\rho c_P)_w \mathbf{u} \nabla T + HS + A \tag{3}$$

where **u** is the Darcy flux ($m \cdot s^{-1}$), **g** the gravitational acceleration (9.81 $m \cdot s^{-2}$), p the pressure (Pa), z the depth (m, positive below ground surface), T the absolute temperature (K), t the time (s), ρ the density ($kg \cdot m^{-3}$), K the intrinsic permeability (m^2), μ the dynamic viscosity (Pa·s), c_p the specific heat ($J \cdot K^{-1} \cdot kg^{-1}$), k the thermal conductivity ($W \cdot m^{-1} \cdot K^{-1}$), *HS* and *A* are the heat source terms ($\mu W \cdot m^{-3}$) due to the magmatic intrusion and the radiogenic heat production of crustal rocks, respectively. The subscripts *r* and *w* refer to the porous rock and water properties, respectively. In the definition of the convective problem, the Boussinesq approximation is assumed. Then, the density variations have a negligible effect on the fluid volume via conservation of mass, which reduces to the condition of incompressibility.

The magmatic body is integrated into the numerical model as a heat source term *HS* ($W \cdot m^{-3}$), whose magnitude varies with time, being proportional to the difference between the magmatic emplacement temperature and that of the surrounding rocks. The temperature of the magmatic body increases almost instantaneously to the imposed magmatic temperature T_{mag} (K) and, accounting for a likely rate of replenishment from below, it is taken constant during a discrete time interval of 49 kyr (from t_1 = 1 kyr to t_2 = 50 kyr). To accomplish this, a time, dependent, rectangular-shaped pulse function $f(t)$ is adopted. As the definition of boundary conditions, that vary abruptly with respect to time, can be difficult to solve numerically, the pulse function $f(t)$ is smoothed by means of a transition window 500-yr wide and centred on ($t_1 - \Delta t/2$) and ($t_2 + \Delta t/2$). This allows us to achieve the emplacement temperature T_{mag} as well as to stop the magmatic replenishment phase in one time-step. The heat source term is scaled by the volumetric heat transfer coefficient, δ_{ht} ($W \cdot m^{-3} \cdot K^{-1}$), defined as the product of the heat transfer coefficient α ($W \cdot m^{-2} \cdot K^{-1}$) to the interfacial

area a (m^{-1}). Experimental heat flux measurements, obtained at liquidus-subliquidus temperatures for basaltic lavas by means of convective heat flux probes (Hardee and Dunn, 1981), constrain the value of α around 0.1 $W \cdot m^{-2} \cdot K^{-1}$. Concerning the interfacial area, it can be interpreted as the total contact area between solid and fluid phases, divided by rock matrix volume. Its value depends on many factors, such as pore shape, size and concentration of the fluid phase. Image processing studies (Garfi *et al*., 2019; Hussaini and Dvorkin, 2020; Scanziani *et al*., 2020) give a wide range of the a value, from less than 0.01 mm^{-1} to more than 10 mm^{-1}. However, the large uncertainty in defining the above-mentioned parameters does not affect the numerical solutions as they play an effective role only in the internal time-steps of the solver.

The further heat source term corresponds to the radiogenic heat production A ($\mu W \cdot m^{-3}$). It is accounted for by an exponential distribution model (Lachenbruch, 1970) with a drop-off length D_A of 10 km (Lachenbruch, 1968) and values assigned by lithology (Morgan, 1985; Verdoya *et al.*, 1998). The constitutive laws describing the heat source terms *HS* and *A* are displayed in Table 2.

Regarding the boundary conditions (Fig. 1B), a stationary air temperature (T_o) and atmospheric pressure (P_o) are set at the ground surface as function of the topographic elevation following the U.S. Government Printing Office (1976). The upper boundary is open to the fluid flow with the implicit assumption that groundwater table coincides with the ground surface. The regional fluid flow is defined by setting on the vertical sides of the model a hydraulic head (h_o) proportional to the topography elevation. Due to the temperature boundary condition adopted for the top surface, cold water enters the system in areas of high topographic relief, i.e. the recharge areas set at the sides of the geothermal reservoir. Indications of a decreasing permeability with depth (Manning and Ingebritsen, 1999) support the assumption of an impermeable lower boundary. Few exposed locations on Earth, e.g. the Ivrea-Verbano Zone (IVZ) in Southern Alps (Italy), allow the study of archetype of continental crust. In the IVZ, petrological studies suggest that lower continental crust consists of highly variable amphibolite to granulite facies rocks (e.g. Schmid and Wood, 1976; Hunziker and Zingg, 1980; Sills, 1984; Pittarello *et al*., 2012). At pressures of 0.8-0.9 GPa, which are typical of crustal levels 25-30 km deep, the equilibrium temperatures are in the interval of 550-700 °C and greater than 650-700 °C, for amphibolite and granulite metamorphic facies, respectively (e.g. Turner, 1968; Wright, 1989). According to the above-mentioned pieces of evidence, a fixed basal temperature, T_{basal} = 650 °C, is set at the bottom of the numerical domain, reflecting the average thermal condition at the base of a continental crust 26 km thick. The lateral boundaries are thermally and hydraulically insulating. These assumptions do not affect the numerical results of the model, whose sides are far enough from the heat source. The time-dependent simulations are initialised assuming a conductive, steady-state temperature distribution without the magmatic heat source and a hydrostatic pressure regime (model 1 of Table 1).

2.3. Transport properties of the rocks and melts

The physical properties of the porous rocks are defined according to *in-situ* conditions, i.e. depth and temperature. The rocks are modelled as a homogeneous, downward anisotropic material by applying the set of constitutive laws displayed in Table 2. The physical parameters are defined by lithothermal units as displayed in Tables 3 and 4.

Table 2 - The constitutive laws used to describe the macroscopic behaviour of the magmatic heat source and the porous rocks.

Property	Constitutive law	Reference
Magmatic heat source	$HS = \delta_{ht} \cdot (T_{mag} - T) \cdot f(t)$	Gola *et al.* (2017)
	$f(t) = \begin{cases} 1 & t_1 \le t \le t_2 \\ 0 & otherwise \end{cases}$	
Radiogenic heat production	$A = A_o \cdot exp(-z/D_A)$	Lachenbruch (1970)
	with D_A = 10 km	
Porosity	$\phi = \phi_o exp(-\beta \cdot z) + \phi_{irr}$	Sclater and Christie (1980)
Rock thermal conductivity	$k_r = k_m^{(1-\phi)} \cdot k_w^{(\phi)}$	Pasquale *et al.* (2011)
	$k_m = k_L + k_R$	This work
	$k_L = \left[k_M + \left(\frac{T_{ref} \cdot T_M}{T_M - T_{ref}}\right) \cdot (k_{mo} - k_M) \cdot \left(\frac{1}{T} - \frac{1}{T_M}\right)\right]$	Sekiguchi (1984)
	with T_{ref} = 293 K, k_M = 1.8418 W m^{-1} K^{-1} and T_M = 1473 K	
	$k_R = \left[\frac{16}{3}\frac{n^2}{\varepsilon}\sigma T^3\right]$	Shatz and Simmons (1972)
	with σ = 5.67 × 10^{-8} W m^{-2} K^{-4}	
Rock thermal capacity	$(\rho c_P)_r = (1 - \phi) \cdot (\rho c_P)_m + \phi \cdot (\rho c_P)_w$	Pasquale *et al.* (2011)
	$(c_P)_m = \sum_{i=1}^{4} (c_P)_{mo} \cdot a_i T^{i-1}$	
	with a_1 = 0.953, a_2 = 2.29 10^{-3}, a_3 = −2.83 10^{-6}, a_4 = 1.19 10^{-9}	
Magma thermal capacity	$(c_P)_{HS} = (c_P)_m + \frac{L}{(T_{liq} - T_{sol})}$	Carslaw and Jaeger (1959)
Magma density	$\rho_{HS} = \rho_{sol} - \frac{\rho_{sol} - \rho_{liq}}{T_{liq} - T_{sol}} \cdot (T - T_{sol})$	This work
	when $T_{sol} \le T \le T_{liq}$	
Magma thermal conductivity	$k_{HS} = k_{sol} - \frac{k_{sol} - k_{liq}}{T_{liq} - T_{sol}} \cdot (T - T_{sol})$	This work
	when $T_{sol} \le T \le T_{liq}$	
Rock permeability	$K_r = K_o \cdot exp(-z/D_K)$	Ebigbo *et al.* (2014)
	with D_K = 2.5 km	

The pore-filling water has a lower conductivity and a higher volumetric heat capacity than the rock-forming minerals, so that the effective thermal properties are very sensitive to the porosity fraction. According to Sclater and Christie (1980), the porosity is assumed to decrease exponentially with the burial depth z (km) from a superficial porosity ϕ_o to an irreducible porosity, ϕ_i. The decreasing rate is defined by the compaction coefficient β (km^{-1}). A common value of the irreducible porosity, ϕ_i = 0.005, is assumed.

The effective rock thermal conductivity k_r (W·m^{-1}·K^{-1}) is computed by the geometrical mean model (Clauser and Huenges, 1995; Pasquale *et al.*, 2011) combining the temperature-dependent thermal conductivity of the rock matrix, k_m, and of the water, k_w, with the depth-dependent porosity. The matrix thermal conductivity is modelled as the sum of the lattice, k_L, and radiative, k_R. components. The temperature dependence of k_L, is accounted for by the equation proposed

by Sekiguchi (1984), which defines a non-linear decreasing trend as function of T^{-1}. Although k_L prevails over the typical temperature range of the upper crust, k_R becomes significant for $T > 500$-700 °C (Birch and Clark, 1940; MacPherson and Schloessin, 1982) due to its T^3 dependence (Shatz and Simmons, 1972; Clauser, 2009). The radiative term balances and sometimes even reverses the decreasing trend of k_L. In order to quantify k_R, the thermal behaviour of the orthopyroxene (enstatite) and quartz minerals, together with their refractive index and absorption coefficient values, are assumed as representative mineralogical constituents of the lower and upper crust, respectively (Wang and Currie, 2015). In Fig. 2 the thermal conductivity measured on single crystals of enstatite and quartz in the 300-1500 K temperature interval (Hofmeister *et al*., 2014) is displayed together with the modelled lattice and radiative components. At about 1000 K, the radiative component is 0.3 and 0.4 $W \cdot m^{-1} \cdot K^{-1}$ for the orthopyroxene and quartz, respectively, and it increases to 0.7 and 1.2 $W \cdot m^{-1} \cdot K^{-1}$ at a temperature of 1400 K.

Table 3 - The physical parameters of the rocks used to compute the thermal models. ϕ_o is the superficial porosity, β the compaction factor, k_{mo} the rock matrix thermal conductivity at ambient conditions, n the refractive index, ε the absorption coefficient, ρ_m the rock matrix density, $c_{p\,mo}$ the rock matrix specific heat at ambient conditions, K_o the superficial permeability, and A_o the superficial radiogenic heat production.

Unit	ϕ_o (-)	β (km^{-1})	k_{mo} ($W\ m^{-1}\ K^{-1}$)	n (-)	ε (cm^{-1})	ρ_m ($kg\ m^{-3}$)	$c_{p\,mo}$ ($J\ K^{-1}\ kg^{-1}$)	K_o (m^2)	A_o ($\mu W\ m^{-3}$)
1	0.400	0.293	2.0	1.544	17	2300	800	10^{-18}	2.0
2	0.250	0.284	4.0			2500	750	$10^{-15} – 10^{-13}$	1.5
3	0.050	0.400	3.2			2650	850	10^{-16}	3.5
4	0.050	0.400	3.7	1.650	30	2800	900	10^{-16}	0.4

Table 4 - The physical parameters of the magmatic body used to compute the thermal models. k is the thermal conductivity, ρ the density, and c_p the specific heat, referred to the solid and melting temperature T, L is the latent heat of crystallisation, α the heat transfer coefficient, and a the interfacial area.

Unit		T (°C)	k ($W\ m^{-1}\ K^{-1}$)	ρ ($kg\ m^{-3}$)	c_p ($J\ K^{-1}\ kg^{-1}$)	L ($kJ\ kg^{-1}$)	α ($W\ m^{-2}\ K^{-1}$)	a (m^{-1})
5	solid	650	3.2	2650	1340	250	0.1	250
	melt	850	1.0	2250	1350			

The effective volumetric heat capacity of the rocks, defined as the product of the specific heat c_p ($J \cdot kg^{-1} \cdot K^{-1}$) to the density ρ ($kg \cdot m^{-3}$), is calculated according to Kopp's law as the arithmetic mean of the individual matrix and fluid contributions weighted by their volume fractions. The temperature dependence of the matrix specific heat is accounted for by a third order polynomial relationship (Pasquale *et al*., 2011), while the temperature effect on the matrix density is neglected, as the thermal expansion of geological materials is small (~10^{-5} $°C^{-1}$). In Fig. 2 the effective thermal properties profiles across the crustal section are displayed assuming a reference

temperature distribution as computed by the steady-state thermal model (model 1 of Table 1).

Real porous media are hydraulically heterogeneous. Nevertheless, in some cases, this heterogeneity might be sufficiently small-scale and statistically random that a single bulk permeability is a reasonable description of the medium. It is straightforward to account for basic permeability variations by simply allowing the permeability to vary spatially, especially along the vertical axis. Here, the effective rock permeability, K_r (m^2), is assumed to decrease as function of burial depth following an exponential trend with a drop-off length D_K of 2.5 km (Ebigbo *et al.*, 2014). In particular, the reservoir permeability is defined by superficial values of $1.0 \cdot 10^{-15}$, $1.0 \cdot 10^{-14}$ and $1.0 \cdot 10^{-13}$ m^2, giving an average reservoir permeability, in the depth interval 1-4 km b.s.l., of $3.9 \cdot 10^{-16}$, $3.9 \cdot 10^{-15}$ and $3.9 \cdot 10^{-14}$ m^2, respectively. The low-permeability units, corresponding to the shallow cap-rock and the basement rocks (upper and lower crust), have a superficial permeability of $1.0 \cdot 10^{-18}$ m^2 and $1.0 \cdot 10^{-16}$ m^2, respectively.

The magmatic body is supposed to be rhyolitic in composition. Rhyolitic melts may have a wide range of melting temperatures (750-1000 °C) but most rhyolites are nearly completely liquid at temperatures above 870 °C and solid below 570 °C. According to Dini *et al*. (2005), crustal melts are emplaced under lithostatic conditions in the Tuscan Magmatic Province (Italy) for temperatures close to 850 °C. In this work, an average melting and solidification points of 850 and 650 °C, respectively, are assumed. Furthermore, according to Lesher and Spera (2015), the density, the specific heat, and the lattice thermal conductivity of typical rhyolitic melts, bearing 2 wt% of dissolved water, are 2250 $kg \cdot m^{-3}$, 1600 $J \cdot kg^{-1} \cdot K^{-1}$, and 1.0 $W \cdot m^{-1} \cdot K^{-1}$, respectively. Below

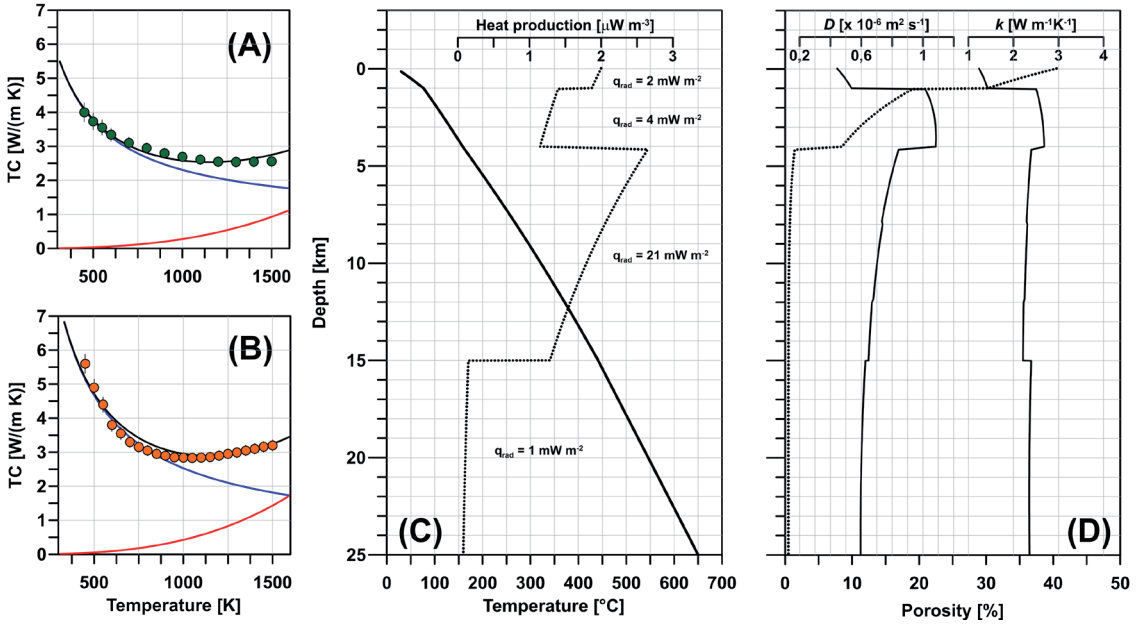

Fig. 2 - Physical properties of the crust: A) the experimental (green circles) and modelled (black line) thermal conductivity values of orthopyroxene crystal at high temperatures; B) the experimental (orange circles) and modelled (black line) thermal conductivity values of quartz at high temperatures. The modelled radiative (red) and lattice (blue) components of thermal conductivity are also displayed; C) the temperature (continuous line) and the radiogenic heat production (dotted line) profiles, corresponding to the initial conditions of the time-dependent models. The amount of the radiogenic heat production within each lithothermal unit is reported; D) the porosity (dotted line), thermal conductivity (continuous line on the right side), and thermal diffusivity (continuous line on the left side) profiles accounting for the *in-situ* conditions (depth and temperature).

the solidification temperature, the thermal properties of the magmatic body are assumed to match those of the upper crustal rocks (unit 3). When the temperature of the cooling magmatic body belongs to its interval of crystallisation, the density and the lattice thermal conductivity vary linearly between those of the melt and the solid rock. The latent heat of crystallisation is about 250-300 kJ·kg^{-1}, then, an additional amount of heat, corresponding to 1250 J·°C^{-1}, is released to the surrounding rocks when the temperature of the magmatic body decreases from 850 to 650 °C. The heat of crystallisation L (kJ·kg^{-1}) is modelled by adding the distributed portion of the latent heat to the effective specific heat (Carslaw and Jaeger, 1959). The physical properties of the magmatic body are displayed in Table 4.

3. Results

3.1. Thermal conduction

Preliminary time-dependent conductive models (models 2a and 2b of Table 1) are solved to study the evolution of the thermal structure by varying the topology and the emplacement depth of the magmatic heat source. It must be emphasised that these conductive models do not consider the growth of the magma chamber or pluton, neither as the cooling facilitated by the fluid circulation. Nonetheless, they are useful as baselines against which the thermal evolution of the more dynamic hydrothermal models can be compared.

In Fig. 3 the time-temperature curves at selected control points display the evolution of the thermal structure in absence of permeable geological units, when the thermal diffusion is the dominant process. Three main phases are distinguishable: an initial heating phase, a quick cooling phase evolving toward a final slow cooling phase. As soon as the magmatic event ends (t_2 = 50 kyr), the temperature at the centre of the magmatic body and at the rock-melt interface decreases by conductive cooling following an exponential trend. Instead, the diffusion of the thermal wave in the surrounding rocks increases the temperature. The thermal signal migrates upwards according to the thermal time constant $\tau = d^2/D$, where d is the distance (m) and D the thermal diffusivity (m^2·s^{-1}). During the cooling phase, a detectable positive thermal anomaly persists even for very long times.

The effect of the latent heat is not negligible as it affects both the cooling history of the magmatic body and the temperature distribution above it. As the latent heat provides energy to the system, the cooling rate is lower. Ignoring this additional heat leads to a slightly cooler temperature in the surrounding region and a somewhat shorter life of the magmatic intrusion. The results show that the temperatures in the overlying hosting rocks are 50 to 100 °C higher and the crystallisation times are 60 to 70 kyr longer in comparison to the models where the latent heat is not accounted for.

3.2. Hydrothermal convection

The presence of a geothermal gradient leads to the formation of a density stratification in the pore-filling water column, with less dense warm water lying below denser cold water. Such a stratification is unstable: if a parcel of fluid is raised slightly, it will experience a weaker downward buoyancy force than its neighbours and will continue to rise. The fluid motion that ensues is called thermal convection. Not all density, or thermal, gradients lead to convection: the dissipative action of the fluid viscosity and the thermal diffusion of temperature act to inhibit convective motion. The comparison of the strength of the buoyancy forces with these dissipative effects gives rise to a

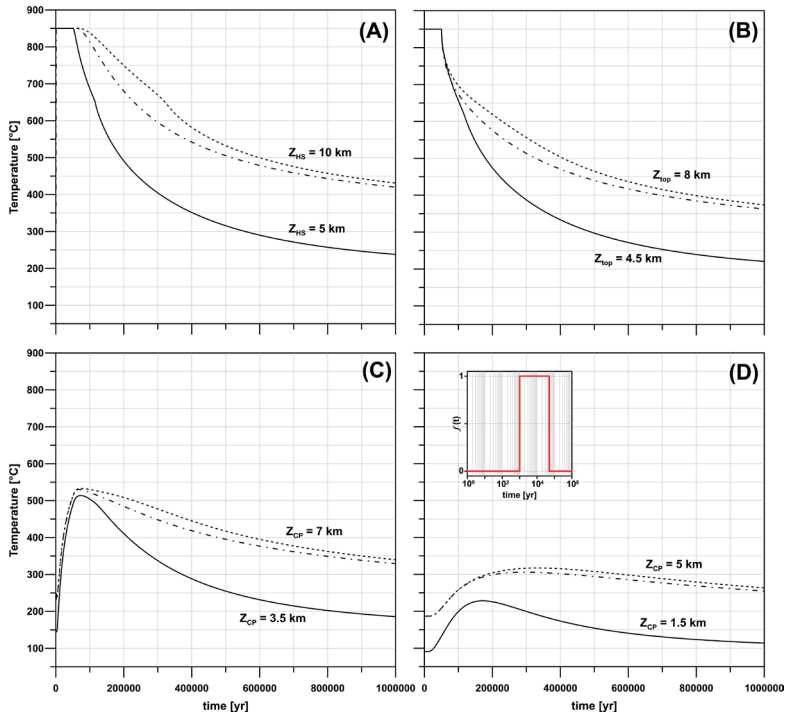

Fig. 3 - Conductive heating and cooling of a magmatic body and hosting rocks. The temperature evolution at four control points set at centre of the magmatic body (A), at its top (B), 1 km above (C) and 3 km above (D). The heat source has a characteristic emplacement depth Z_{HS} = 5 km b.s.l. (continuous line) and Z_{HS} = 10 km b.s.l. (dashed line) with a vertical axis of 1 and 4 km, respectively, and an emplacement temperature T_{mag} = 850 °C. The dashed-dotted line corresponds to the temperature evolution evaluated without considering the latent heat of crystallisation, for the scenario having an emplacement depth of 10 km. The inset figure in panel D display the pulse function *f*(t) defining the time interval during which the heat source is active (t_1 = 1 kyr and t_2 = 50 kyr).

dimensionless ratio known as the Rayleigh number, *Ra*. If the Rayleigh number is small, dissipative forces act to inhibit convection, whereas if it is large, buoyancy forces dominate and drive strong convective flow. When the boundary conditions consist of a basal heat flow, and fixed temperature and fluid pressure at the top, the Rayleigh number is given as (Nield and Bejan, 2006):

$$Ra = \frac{\left(\rho_o \, c_p \, \rho \, \beta\right)_w \, \mathbf{g} \, \mathbf{q} \, K_r \, H^2}{\mu_w \, k_r^2} \tag{4}$$

where ρ_o, c_p, ρ, β and μ are the reference density (ρ_o = 1000 kg·m^{-3}), the temperature-dependent heat capacity, density, thermal expansion and dynamic viscosity of the fluid, respectively, **g** is the gravity, **q** the heat flow at the base of the system, *H* the length scale of the system (equals to the reservoir thickness), K_r and k_r are the effective permeability and thermal conductivity of the reservoir, respectively.

In an infinitely-extended horizontal porous layer uniformly heated from the below and cooled from above, when *Ra* exceeds the critical value of $4\pi^2$ (*Ra* ≈ 40), the conductive regime becomes unstable and the fluid flow starts to exhibit convective structures. The domain aspect ratio, i.e. the ratio of the horizontal (*W*) to the vertical (*H*) dimension of the Rayleigh-Darcy domain, may significantly affect the convective pattern. When *W*/*H* is smaller than the smallest unstable

wavelength $\lambda = 4\pi/\left(\sqrt{Ra} + \sqrt{Ra - 4\pi^2}\right)$, no convection occurs due to the stable conduction state (Horton and Rogers, 1945). To obtain reliable results, the Rayleigh-Darcy domain should contain at least one sustained megaplume (Wen *et al*., 2013) and, for $Ra = 4\pi^2$, the horizontal dimension must be at least twice the vertical one ($\lambda = 2$). This condition is met as the aspect ratio of the modelled geothermal reservoir is 5 ($\overline{W}$ = 15 km, H = 3 km).

In Fig. 4 the *Ra* numbers, calculated by Eq. 4 at every time-step using the surface-averaged parameters relative to the reservoir domain, are displayed for different boundary conditions,

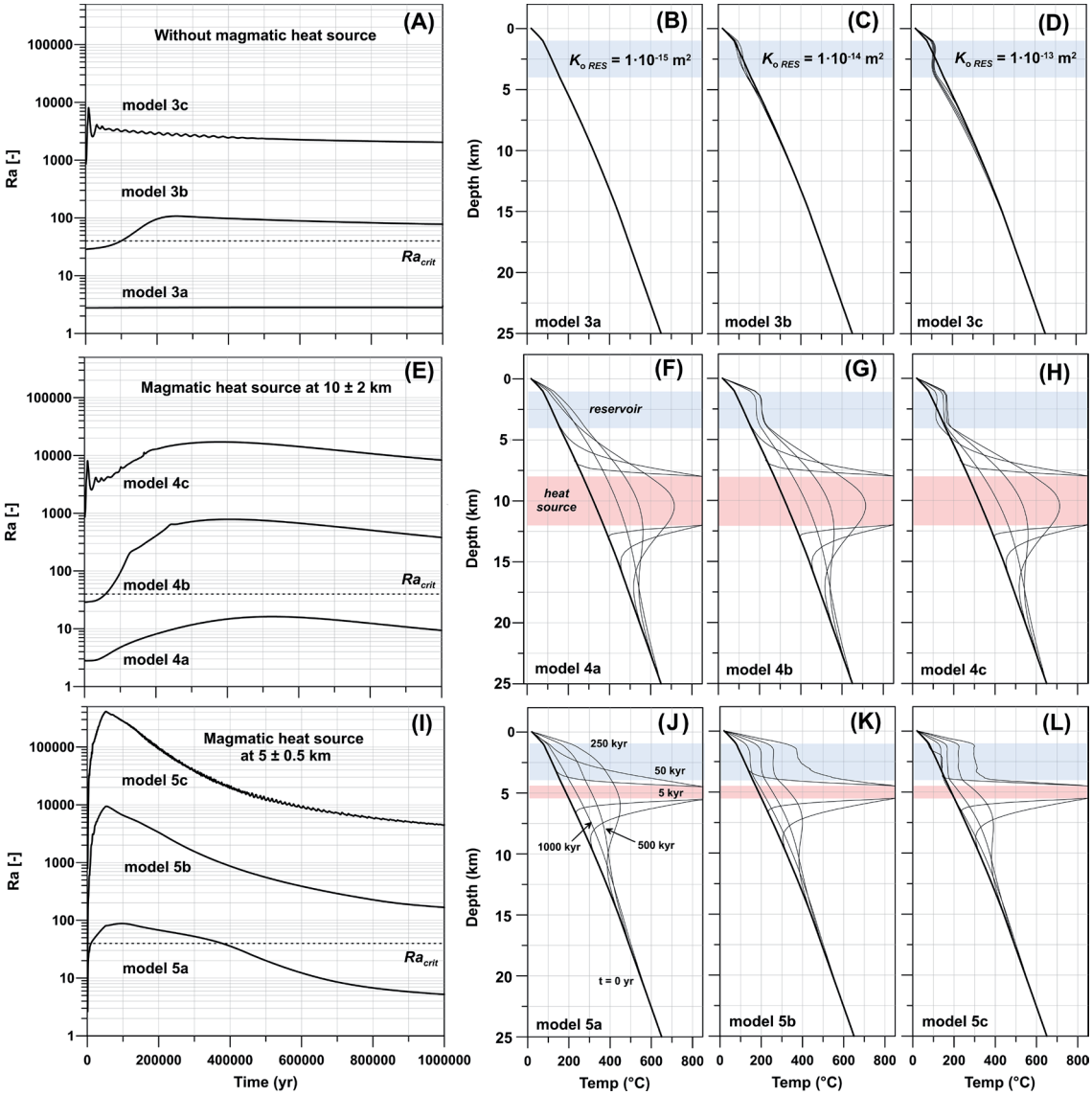

Fig. 4 - Averaged Rayleigh number and conductive-convective temperature profiles. The evolution of the *Ra* number, computed at each time-step of the time-dependent models, for the scenarios involving a reservoir heated from below by a regional heat flow (A), a magmatic body 10 km deep (E) and 5 km deep (I) is displayed. The vertical temperature profiles, crossing the models at the middle point of the horizontal distance, are also displayed for selected times (5, 50, 250, 500, and 1000 kyr) and for the scenarios involving a reservoir heated from below by a regional heat flow (B to D), a magmatic body 10 km deep (F to H) and 5 km deep (J to L). See Table 1 for details of the model parameters.

together with the vertical temperature profiles at selected time-steps, evaluated at the middle point of the horizontal distance. First, the thermal structure is resolved for the more general situation corresponding to a geothermal reservoir heated from below and neglecting the magmatic heat source (models 3a to 3c of Table 1). Successively, the magmatic heat sources, 10 and 5 km deep, are considered (models 4a to 4c and 5a to 5c of Table 1, respectively). The reservoir permeability, as well as the heat flow at the base of the reservoir domain, provide the main constraints on the size of the Rayleigh number. As the temperature gradient, or the heat supplied to the system, is increased, the convection pattern undergoes transitions to new modes of behaviour. The heat transport in low-permeability rocks (K_{RES} ~ 10^{-16} m^2) is unlikely to be convective, even when a deep magmatic body occurs, as displayed in the models 3a (Ra = 3) and 4a (Ra = 3-16). Instead, in presence of a relatively shallow magmatic body, the heat carried out by the motion of the geothermal fluids defines convex-upward temperature profiles, as displayed in the model 5a (Ra = 3-88). Nevertheless, the vertical temperature profiles of models 3a, 4a, and 5a do not display isothermal sections. Instead, the transition to well-defined convective patterns, characterised by isothermal sections or even temperature reversals, occurs when the effective reservoir permeability assumes medium-to-high values (K_{RES} ~ 10^{-15}-10^{-14} m^2), as displayed in all the remaining models.

In Fig. 5 the 2D temperature distributions relative to the high-permeability models (3c, 4c, and 5c of Table 1) are displayed at selected time-steps, corresponding to the early and late magmatic stages (5 and 50 kyr, respectively), and the middle and late cooling stages (250 and 500 kyr, respectively). As a rule, the onset of the thermal convection is a time-dependent process, whose occurrence depends on the initial thermal conditions and rock permeability. The large-scale

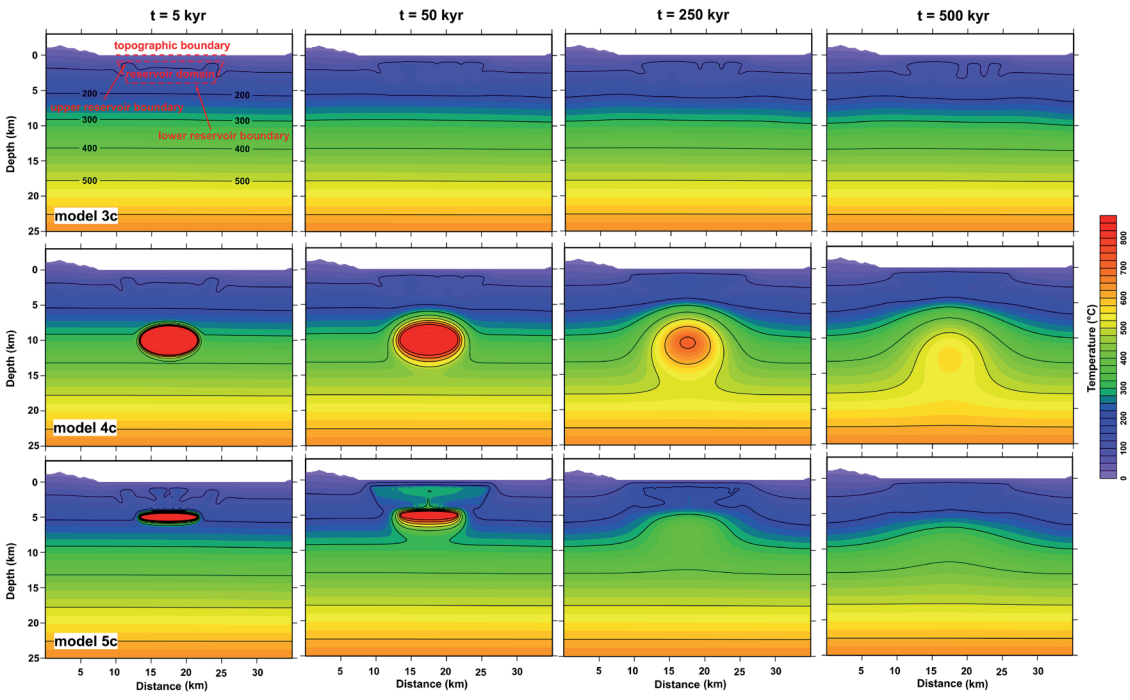

Fig. 5 - 2D conductive-convective thermal models. Time-dependent temperature distributions computed with and without the presence of a magmatic heat source. See Table 1 for details of the model parameters. The dashed lines in the upper-left panel indicate the boundaries and the domain on which the heat flow and temperature values of Fig. 6 are averaged.

convective cells develop after few hundred or thousand years. In magmatic environments, the onset of a more vigorous thermal convection rests on the time required to the thermal pulse to migrates upwards from the magmatic heat source to the lower boundary of the reservoir. As soon as the magmatic thermal input warms the reservoir rocks, the large convective flow transports the thermal energy from the base to the top boundaries of the reservoir domain faster than the energy can be dissipated conductively through the impervious cap-rock unit. This condition determines vigorous horizontal fluxes at the top of the permeable layer, which control the lateral extension of the thermal plume.

4. Transient effects on the surface heat flow and reservoir temperature

Heat is continuously transported from the Earth's interior towards its outer surface. Measurement of the heat flow provides important constraints on temperatures at depth. In this context, the heat transfer from the top of the reservoir units to the surface occurs via thermal diffusion, due to the low permeability value of the caprock unit. The transient tectono-magmatic and hydrothermal processes are responsible of the surface heat flow variations, whose magnitudes are function of space, time and hydraulic properties of the underlying permeable units.

In Fig. 6, the temporal evolution of the surface heat flow, with its maximum and minimum values, the top and bottom reservoir temperatures as well as the average reservoir temperature, are displayed for the different model scenarios. The analysed quantities are averaged values. In detail, the surface heat flow and the reservoir top and bottom temperatures correspond to the spatially averaged values along the 1D topographic, upper and lower reservoir boundaries, respectively; instead, the average reservoir temperature corresponds to the surface averaged values relative to the 2D reservoir domain, as displayed in Fig. 5.

The steady-state conductive model gives an initial heat flow of 70 $mW \cdot m^{-2}$; an average reservoir temperature of 116 °C, with bottom and top temperatures of 156 and 75 °C, respectively. Small variations of the heat flow (±6 $mW \cdot m^{-2}$) depend on the isotherm refraction due to topographic irregularities and subsurface thermal conductivity contrasts. The thermal convection, triggered by the regional thermal gradient (models 3b and 3c of Table 1), is responsible for the growing surface heat flow up to 80 and 100 $mW \cdot m^{-2}$, for an effective reservoir permeability of the order of 10^{-15} and 10^{-14} m^2, respectively. Large deviations from the average heat flow value, both in the positive and negative directions, occur where the convective currents define up-welling and down-welling zones, respectively. The transient nature of the thermal convection is well recognisable and the time at which the convection starts decreases with the increasing permeability. The thermal convection homogenises the reservoir temperature, so that the temperature differences between top and bottom boundaries decrease with time, until a stable convection is reached.

The magmatic input (models 4a to 4c and 5a to 5c) determines higher average heat flow values at surface of the order of 200-300 $mW \cdot m^{-2}$, with picks up to 450 $mW \cdot m^{-2}$ at the early-stage of the magmatic phase and for a reservoir permeability of the order of 10^{-14} m^2. The mid-crustal magmatic body (10 km deep) warms the geothermal fluids up to 250 °C in the deepest section of the reservoir. Nevertheless, the average reservoir temperatures grow to maxima values in the interval 150-180 °C. In order to have high-temperature geothermal fluids available, the emplacement of upper-crustal plutons is required. Shallow plutons are capable to warm the geothermal fluids up to an average reservoir temperature of 260-280 °C.

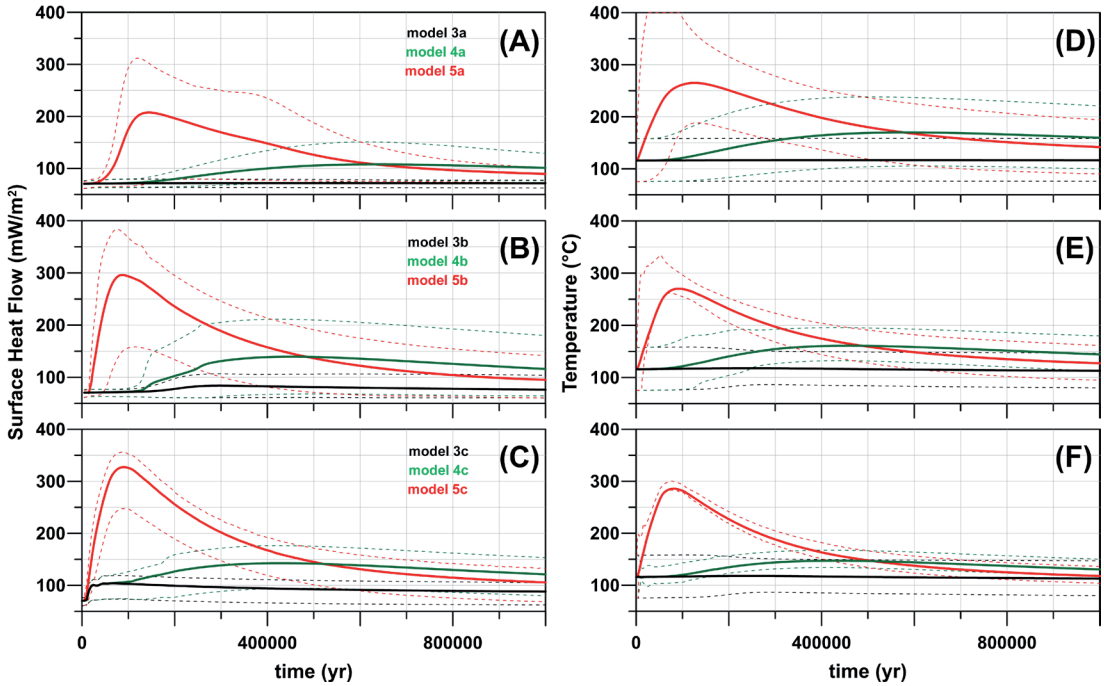

Fig. 6 - Temporal variations of surface heat flow and reservoir temperature. The time-dependent heat flow values (continuous line) averaged over the topographic boundary overlying the geothermal reservoir (see Fig. 5), together with the maximum and minimum values (dashed line), evaluated for the low (A: $K_{o\,RES} = 1{\cdot}10^{-15}$ m^2), medium (B: $K_{o\,RES} = 1{\cdot}10^{-14}$ m^2) and high (C: $K_{o\,RES} = 1{\cdot}10^{-13}$ m^2) reservoir permeability models. The time-dependent temperature values (continuous line) averaged over the reservoir domain (see Fig. 5), together with the temperatures averaged over the lower and upper reservoir boundaries (dashed line), evaluated for the low (D), medium (E) and high (F) reservoir permeability models. The curves refer to the model results corresponding to the scenarios without the magmatic heat source (black line), with the magmatic heat source 10 km deep (green line) and 5 km deep (red line). See Table 1 for details of the model parameters.

Nevertheless, the intrinsic transient nature of the magmatic hydrothermal systems, confines their life-time to few hundred thousand years, with thermal pick limited to the early-stage of the magmatic phase. Locally, thermal convection is capable to transport towards the upper boundary of the reservoir high-temperature fluids up to 180-280 °C. Conductive heat transfer from a magmatic intrusion to the surrounding groundwater occurs in the roots of the geothermal system below the depth of typical conventional geothermal wells. The modelling results suggest that superhot geothermal fluids, with temperatures exceeding ~400 °C, may exist at the boundary between geothermal systems and the magmatic heat source.

5. Conclusions

The nature of heat and fluid transport in continental setting, also accounting for the role of deep-seated magmatic intrusions, has been analysed numerically by a series of heuristic models able to describe the general features of many hydrothermal systems. With the aim of studying the style and magnitude of the fluid circulation together with its thermal effects, the hydrothermal system has been investigated for a variety of rock permeability, magma emplacement depth, and topology of the magmatic heat source. Although the selected variables do not cover the whole

spectrum of the physical parameters characterising the hydrothermal systems, they represent the key variables controlling the subsurface temperature distribution as well as the rheological stratification in magmatic environments, as it has been highlighted in former studies in volcanic areas like Ischia Island (Castaldo *et al*., 2017) and Long Valley Caldera (Gola *et al*., 2021).

Prior conductive models pointed out the key role of the latent heat of crystallisation in the definition of the magnitude and life-time of the thermal anomaly induced by the magmatic heat source. Neglecting the amount of heat released during the crystallisation of the magmatic body, the temperatures in the vicinity of the intrusion should be underestimated up to 50 °C and, even more important, the cooling time shortened up to 70 kyr. Both temperature and time are essential parameters in contact metamorphism studies. They control the thermal peak recorded by the hosting rocks overlying a magmatic intrusion as well as the thickness of the thermal aureole. In this context, the modelling of thermal evolution as function of the distance from the heat source may be a valuable technique to unravel the magmatic emplacement depth and temperature as well as the timing and the duration of the magmatic input. However, when the petrological and geochronological information from core samples are integrated with the numerical results, any uplift and erosion effects must be considered. As a matter of fact, the actual position (i.e. the depth) of the core samples may not coincide with the original one at the time of the intrusion, as indicated by Dallmeyer and Liotta (1998) for the case of the long-lived magmatic system of Larderello (Tuscany, Italy).

The convective models show that the large heat flow from the heat source triggers a vigorous thermal convection when the rock permeability is larger than 10^{-16} m^2. In the absence of a heat source of magmatic origin, thermal convection requires rock permeabilities larger than 10^{-15} m^2. In these conditions, the spatial redistribution of thermal energy notably differs from a purely conductive thermal model. In fact, the permeability provides one of the main constraints on the size of the Rayleigh number, which, in the magmatic geothermal systems, can assume values of the order of 10^3-10^5, well beyond its critical value. Furthermore, the time-dependent models show three distinct stages: 1) an early-stage, during which conduction dominates meanwhile the *Ra* number grows to the critical value, 2) a middle-stage, during which an array of plumes rapidly grows above the lower surface, and 3) a late-stage, during which large-scale convection cells appear and, gradually, the layer becomes dominated by the buoyancy forces.

The hottest hydrothermal plumes and high surface heat flow values are associated with rather higher permeability (Figs. 6a to 6c). When magma intrudes and heats host rock, uniformly "high" reservoir permeabilities (approximately ≥ 10^{-14} m^2, models 4c and 5c) lead to relatively low heat flow values because heat advects rapidly away from the magma reservoir. "Low" permeability values (approximately ≤ 10^{-16} m^2, models 4a and 5a) also lead to lower heat flow values, in this case because the thermal regime is conduction-dominated. Intermediate permeability ($\sim 10^{-15}$ m^2, models 4b and 5b) lead to the highest surface heat flow values. When the crust undergoes thermal perturbation of magmatic origin, the time necessary to return to its initial thermal equilibrium is long, so that the temperature and heat flow anomalies (Figs. 4 and 5) are still detectable after several hundred thousand years. In order to have high-temperature geothermal fluids at economically drillable depths, with temperatures above 200 °C, or similarly with surface heat flow values larger than 150 mW·m^{-2}, the emplacement of young (<< 1 Myr) upper-crustal (< 5-10 km) plutons is required. These pieces of evidence are in agreement with the main outcomes reported by Rochira *et al.* (2018). Although the authors performed time-dependent conductive thermal models accounting for the emplacement of a granitic body 3 km deep beneath the Larderello area (Tuscany, Italy), they reproduced the regional heat flow

anomaly of 150-200 $mW \cdot m^{-2}$ invoking an instantaneous magmatic event 0.3 Myr old. Even accounting for an incremental growth of the magmatic intrusion, the observed thermal anomaly can be replicated only in the final stages of pluton accretion at 0.3 Myr by present. This age is considerably lower than the geochronologic dates (3.8-1.3 Myr) available for some intrusive rocks cored in exploratory wells in the Larderello geothermal field [see Gola *et al*. (2017) and references therein for a comprehensive geochronological compilation]. Based on these thermal pieces of evidence, a relatively continuous magmatic activity is required to sustain such as long-lived magmatic geothermal system and the findings of younger granites in future drillings cannot be ruled out.

The present results can be also framed into other real cases, like the high temperature geothermal system beneath the Ischia Island (Castaldo *et al*., 2017). The temperature profiles coming from the deep boreholes in the south-western sector of the island display a typical conductive feature at shallow depth down to about 200-400 m b.g.l. related to an impermeable, mainly argillic, layer acting as caprock. The deeper green tuff and lava formations constitute the deep-seated geothermal reservoir where an isothermal profile at 150-180 °C is observed down to a maximum depth of about 1000 m b.g.l. Below this convective layer, the thermal gradient abruptly increases conductively to a maximum temperature of 225 °C at 1100-1200 m b.g.l. Additionally, water equilibrium temperatures, evaluated by Na-K-Mg geothermometers, in the 240-300 °C range support the hypothesis that the geothermal system of Ischia extends down to greater depths. In such a geological context, a shallow mush magmatic intrusion at about 600 °C with the top located at a depth of about 1.3-1.7 km, as inferred from gravimetric and magnetic modelling, represents the principal heat source. These thermal features mimic the results displayed in Figs. 4 and 6 for the case of the upper crustal pluton.

As final remark, the models presented in this work highlight the main thermal aspects of interest in the geothermal research with possible applications also in other fields, such as the study of magmatic and metamorphic crustal processes. Given the general nature of this study, some specific aspects such as fluid-rock reactions or surface deformations (uplift/erosion) were not considered. This approach represents a reasonable balance between the complexity of real natural systems and the simplifications necessary in the development of physical/mathematical models. The main objective of this work is to investigate and, if applied to natural cases, to replicate the thermal characteristics observable at the surface (heat flow) or at depth (underground temperatures) in a dynamic (time-dependent) context.

REFERENCES

Annen C., Jonathan D., Blundy J.D. and Sparks R.S.J.; 2008: *The sources of granitic melt in Deep Hot Zones.* Trans. R. Soc. Edinburgh: Earth Sciences, 97, 297-309.

Bellani S., Brogi A., Lazzarotto A., Liotta D. and Ranalli G.; 2004: *Heat flow, deep temperatures and extensional structures in the Larderello Geothermal Field (Italy): constraints on geothermal fluid flow*. J. Volcanol. Geotherm. Res., 132, 15-29.

Birch F. and Clark H.; 1940: *The thermal conductivity of rocks and its dependence upon temperature and composition*. Amer. J. Sci., 238, 529-558 and 613-635.

Brogi A., Lazzarotto A., Liotta D. and Ranalli G.; 2005: *Crustal structures in the geothermal areas of southern Tuscany (Italy): insights from the CROP 18 deep seismic reflection lines*. J. Volcanol. Geotherm. Res., 148, 60-80.

Brown G.C. and Mussett A.E.; 1993: *The continental crust*. In: Brown G.C. and Mussett A.E. (eds), The inaccessible Earth: an integrated view to its structure and composition. Springer, Dordrecht, The Netherlands, pp. 186-212.

Carslaw H.S. and Jaeger J.C.; 1959: *Conduction of heat in solids, 2nd ed*. Oxford University Press, London, UK, 520 pp.

Castaldo R., Gola G., Santilano A., De Novellis V., Pepe S., Manzo M., Manzella A. and Tizzani P.; 2017: *The role of thermo-rheological properties of the crust beneath Ischia Island (southern Italy) in the modulation of the ground deformation pattern*. J. Volcanol. Geotherm. Res., 344, 154-173.

Chapman D.S.; 1986: *Thermal gradients in the continental crust*. Geological Society, London, UK, Special Publications, 24, pp. 63-70, doi: 10.1144/GSL.SP.1986.024.01.07.

Chapman D.S., Keho T.H., Bauer M.S. and Picard M.D.; 1984: *Heat flow in the Uinta Basin determined from bottom hole temperature (BHT) data*. Geophys., 49, 453-466.

Chiodini G., Todesco M., Caliro S., Del Gaudio C., Macedonio G. and Russo M.; 2003: *Magma degassing as a trigger of bradyseismic events: the case of Phlegrean Fields (Italy)*. Geophys. Res. Lett., 30, 1434, doi: 10.1029/2002GL016790.

Chiodini G., Avino R., Brombach T., Caliro S., Cardellini C., de Vita S., Frondini F., Marotta E. and Ventura G.; 2004: *Fumarolic and diffuse soil degassing west of Mount Epomeo, Ischia (Italy)*. J. Volcanol. Geotherm. Res., 133, 291-309.

Clauser C.; 2009: *Heat transport processes in the Earth's crust*. Surv. Geophys., 30, 163-191.

Clauser C. and Huenges E.; 1995: *Thermal conductivity of rocks and minerals. Rock physics and phase relations*. In: Ahrens T.J. (ed), Rock Physics and Phase Relations, A Handbook of Physical Constants, AGU Ref. Shelf, Vol. 3, pp. 105-126.

Cloetingh S., van Wees J.D., Ziegler P.A., Lenkey L., Beekman F., Tesauro M., Förster A., Norden B., Kaban M., Hardebol N., Bonté D., Genter A., Guillou-Frottier L., Ter Voorde M., Sokoutis D., Willingshofer E., Cornu T. and Worum G.; 2010: *Lithosphere tectonics and thermo-mechanical properties: an integrated modelling approach for Enhanced Geothermal Systems exploration in Europe*. Earth Sci. Rev., 102, 159-206.

Dallmeyer R.D. and Liotta D.; 1998: *Extension, uplift of rocks and cooling ages in thinned crustal provinces: the Larderello geothermal area (inner Northern Apennines, Italy)*. Geol. Mag., 135, 193-202.

Della Vedova B., Vecellio C., Bellani S. and Tinivella U.; 2008: *Thermal modelling of the Larderello geothermal field (Tuscany, Italy).* Int. J. Earth Sci., 97, 317-332.

Dini A., Gianelli G., Puxeddu M. and Ruggieri G.; 2005: *Origin and evolution of Pliocene–Pleistocene granites from the Larderello geothermal field, Tuscan Magmatic Province, Italy*. Lithos, 81, 1-31, doi: 10.1016/j.lithos.2004.09.002.

DiPippo R.; 2016: *Overview of geothermal energy conversion systems: reservoir-wells-piping-plant-reinjection.* In: DiPippo R. (ed), Geothermal power generation: developments and innovation, Woodhead Publishing, Larderello, Italy, pp. 203-215.

Ebigbo A., Niederau J., Marquart G., Inversi B., Scrocca D., Gola G., Arnold J., Montegrossi G., Vogt C. and Pechnig R.; 2014: *Evaluation of the geothermal energy potential in the medium-enthalpy reservoir Guardia dei Lombardi, Italy*. In: Proc., 39th Workshop on Geothermal Reservoir Engineering Stanford University, Stanford, CA, USA, SGP-TR-202, 7 pp.

Ebigbo A., Niederau J., Marquart G., Dini I., Thorwart M., Rabbel W., Pechnig R., Bertani R. and Clauser C.; 2016: *Influence of depth, temperature, and structure of a crustal heat source on the geothermal reservoirs of Tuscany: numerical modelling and sensitivity study*. Geotherm. Energy, 4, 1-29.

Funnell R., Chapman D., Allis R. and Armstrong P.; 1996: *Thermal state of the Taranaki basin, New Zealand*. J. Geophys. Res., 101, 25197-25215.

Garfi G., John C.M., Berg S. and Krevor S.; 2019: *The sensitivity of estimates of multiphase fluid and solid properties of porous rocks to image processing*. Transp. Porous Media, 131, 985-1005.

Gibert B., Seipold U., Tommasi A. and Mainprice D.; 2003: *Thermal diffusivity of upper mantle rocks: influence of temperature, pressure, and the deformation fabric*. J. Geophys. Res.: Solid Earth, 108, ID2359, doi: 10.1029/2002JB002108.

Gibert B., Schilling F.R., Gratz K. and Tommasi A.; 2005: *Thermal diffusivity of olivine single crystals and a dunite at high temperature: evidence for heat transfer by radiation in the upper mantle*. Phys. Earth Planet. Inter., 151, 129-141.

Gola G., Bertini G., Bonini M., Botteghi S., Brogi A., De Franco R., Dini A., Donato A., Gianelli G., Liotta D., Manzella A., Montanari D., Montegrossi G., Petracchini L., Ruggieri G., Santilano A., Scrocca D. and Trumpy E.; 2017: *Data integration and conceptual modelling of the Larderello geothermal area, Italy*. Energy Procedia, 125, 300-309.

Gola G., Barone A., Castaldo R., Chiodini G., D'Auria L., García-Hernández R., Pepe S., Solaro G. and Tizzani P.;

2021: *A novel multidisciplinary approach for the thermo-rheological study of volcanic areas: the case study of Long Valley Caldera*. J. Geophys. Res.: Solid Earth, 126, e20331, doi: 10.1029/2020JB020331.

Gorczyk W. and Vogt K.; 2018: *Intrusion of magmatic bodies into the continental crust: 3-D numerical models*. Tectonics, 37, 705-723.

Hardee H.C. and Dunn J.C.; 1981: *Convective heat transfer in magmas near the liquidus*. J. Volcanol. Geotherm. Res., 10, 195-207.

Harlov D.E.; 2012: *The potential role of fluids during regional granulite-facies dehydration in the lower crust*. Geosci. Front., 3, 813-827.

Hofmeister A.M., Dong J. and Branlund J.M.; 2014: *Thermal diffusivity of electrical insulators at high temperatures: evidence for diffusion of bulk phonon-polaritons at infrared frequencies augmenting phonon heat conduction*. J. Appl. Phys., 115, 163517, doi: 10.1063/1.4873295.

Horton C.W. and Rogers F.T.; 1945: *Convection currents in a porous medium*. J. Appl. Phys., 16, 367-370.

Hunziker J.C. and Zingg A.; 1980: *Lower palaeozoic amphibolite to granulite facies metamorphism in the Ivrea zone (Southern Alps, northern Italy)*. Schweiz. Mineral. Petrogr. Mitt., 60, 181-213.

Hussaini S.R. and Dvorkin J.; 2020: *Specific surface area versus porosity from digital images*. J. Pet. Sci. Eng., 196, 107773.

Ingebritsen S.E. and Manning C.E.; 2003: *Implication of crustal permeability for fluid movement between terrestrial fluid reservoirs*. J. Geochem. Explor., 78-79, 1-6.

Ingebritsen S.E., Sanford W. and Neuzil C.; 2006: *Groundwater in geologic processes, 2nd ed.* Cambridge University Press, Cambridge, UK, 564 pp.

Ingebritsen S.E., Geiger S., Hurwitz S. and Driesner T.; 2010: *Numerical simulation of magmatic hydrothermal systems*. Rev. Geophys., 48, RG1002.

Jaupart C., Labrosse S., Lucazeau F. and Mareschal J.C.; 2015: *Temperatures, heat, and energy in the mantle of the Earth*. In: Schubert G. (ed), Treatise on Geophysics, 2nd ed., Elsevier, Oxford, UK, Vol. 7, pp. 223-270, doi: 10.1016/B978-0-444-53802-4.00126-3.

Kooi H.; 2016: *Groundwater flow as a cooling agent of the continental lithosphere*. Nature Geosci., 9, 227-230.

Lachenbruch A.H.; 1968: *Preliminary geothermal model of the Sierra Nevada*. J. Geophys. Res., 73, 6977-6989, doi: 10.1029/JB073i022p06977.

Lachenbruch A.H.; 1970: *Crustal temperature and heat production: implications of the linear heat-flow relation*. J. Geophys. Res., 75, 3291-3300, doi: 10.1029/JB075i017p03291.

Lesher C. and Spera F.J.; 2015: *Thermodynamic and transport properties of silicate melts and magma*. In: Sigurdsson H., Houghton B., McNutt S., Rymer H. and Stix J. (eds), The Encyclopedia of Volcanoes, 2nd ed., Elsevier, The Netherlands, pp. 113-142.

Liotta D., Brogi A., Meccheri M., Dini A., Bianco C. and Ruggieri G.; 2015: *Coexistence of low-angle normal and high-angle strike- to oblique-slip faults during Late Miocene mineralization in eastern Elba (Italy).* Tectonophys., 660, 17-34.

Liu J., Xia Q-K., Kuritani T., Hanski E. and Yu H-R.; 2017: *Mantle hydration and the role of water in the generation of large igneous provinces*. Nat. Commun., 8, 1824, doi: 10.1038/s41467-017-01940-3.

MacPherson W.R. and Schloessin H.H.; 1982: *Lattice and radiative thermal conductivity variations through high p, T polymorphic structure transitions and melting points*. Phys. Earth Planet. Inter., 29, 58-68, doi: 10.1016/0031-9201(82)90138-8.

Majorowicz J., Polkowski M. and Grad M.; 2019: *Thermal properties of the crust and the lithosphere-asthenosphere boundary in the area of Poland from the heat flow variability and seismic data.* Int. J. Earth Sci. (Geol. Rundsch.), 108, 649-672, doi: 10.1007/s00531-018-01673-8.

Manning C.E. and Ingebritsen S.E.; 1999: *Permeability of the continental crust: implications of geothermal data and metamorphic systems*. Rev. Geophys., 37, 127-150.

Meissner R.; 1986: *The composition of the continental crust*. In: Meissner R. (ed), The Continental Crust, A Geophysical Approach, International Geophysics Series, Academic Press, Orlando, FL, USA, Vol. 34, pp. 213-241.

Montanari D., Minissale A., Doveri M., Gola G., Trumpy E., Santilano A. and Manzella A.; 2017: *Geothermal resources within carbonate reservoirs in western Sicily (Italy): a review*. Earth Sci. Rev., 169, 180-201.

Morgan P.; 1985: *Crustal radiogenic heat production and the selective survival of ancient continental crust*. J. Geophys. Res.: Solid Earth, 90, C561-C570.

Nield D.A. and Bejan A.; 2006: *Convection in Porous media*, *3rd ed.* Springer, New York, NY, USA, 640 p.

Norton D.; 1977: *Fluid circulation in the Earth's crust*. In: Heacock J.G., Keller G.V., Oliver J.E. and Simmons G. (eds), The Earth's Crust, American Geophysical Union, Washington, D.C., USA, Geophysical Monograph, 20, pp. 693-704.

Norton D. and Knight J.; 1977: *Transport phenomena in hydrothermal systems: cooling plutons*. Amer. J. Sci., 277, 937-981.

Pasquale V., Chiozzi P. and Verdoya M.; 2010: *Tectonothermal processes and mechanical strength in a recent orogenic belt: Northern Apennines*. J. Geophys. Res.: Solid Earth, 115, B3, doi: 10.1029/2009JB006631.

Pasquale V., Gola G., Chiozzi P. and Verdoya M.; 2011: *Thermophysical properties of the Po basin rocks*. Geophys. J. Int., 186, 69-81.

Petford N., Cruden A.R., McCaffrey K.J.W. and Vigneresse J.-L.; 2000: *Granite magma formation, transport andbemplacement in the Earth's crust.* Nature, 408, 669-673.

Pittarello L., Pennacchioni G. and Di Toro G.; 2012: *Amphibolite-facies pseudotachylytes in Premosello metagabbros and felsic mylonites (Ivrea zone, Italy)*. Tectonophys., 580, 43-57.

Ranalli G. and Rybach L.; 2005: *Heat flow, heat transfer and lithosphere rheology in geothermal areas: Features and examples*. J. Volcanol. Geotherm. Res., 148, 3-19.

Rochira F., Caggianelli A. and de Lorenzo S.; 2018: *Regional thermo-rheological field related to granite emplacement in the upper crust: implications for the Larderello area (Tuscany, Italy)*. Geodin. Acta, 30, 225-240.

Santilano A., Manzella A., Gianelli G., Donato A., Gola G., Nardini I., Trumpy E. and Botteghi S.; 2015: *Convective, intrusive geothermal plays: what about tectonics?* Geotherm. Energy Sci., 3, 51-59.

Scanziani A., Lin Q., Alhosani A., Blunt M.J. and Bijeljic B.; 2020: *Dynamics of fluid displacement in mixed-wet porous media*. Proc. R. Soc. A., 476, 20200040, doi: 10.1098/rspa.2020.0040.

Schmid R. and Wood B.J.; 1976: *Phase relationships in granulitic metapelites from the Ivrea-Verbano zone (Northern Italy)*. Contrib. Mineral. Petrol., 54, 255-279.

Sclater J.G. and Christie P.A.F.; 1980: *Continental stretching: an example of the post-mid-Cretaceous subsidence of the central North Sea basin*. J. Geophys. Res., 85, 3711-3739.

Sekiguchi K.; 1984: *A method for determining terrestrial heat flow in oil basinal areas*. Tectonophys., 103, 67-79.

Shatz J. and Simmons G.; 1972: *Thermal conductivity of Earth materials at high temperatures*. J. Geophys. Res., 77, 6966-6983.

Shellnutt J.G. and Thuy T.P.; 2018: *Mantle potential temperature estimates and primary melt compositions of the low-Ti Emeishan Flood Basalt.* Front. Earth Sci., 6, 67, doi: 10.3389/feart.2018.00067.

Sills J.D.; 1984: *Granulite facies metamorphism in the Ivrea zone, N.W. Italy*. Schweiz. Mineral, Petrogr. Mitt., 64, 169-191.

Stein C.A.; 1995: *Heat flow of the Earth.* In: Ahrens T.J. (ed), Global Earth physics - A handbook of physical constants, American Geophysical Union, Washington, D.C., USA, AGU Reference Shelf, Vol. 1, pp. 144-158.

Stober I. and Bucher K.; 2014: *Hydraulic conductivity of fractured upper crust: insights from hydraulic tests in boreholes and fluid-rock interaction in crystalline basement rocks*. Geofluids, 15, 161-178, doi.org/10.1111/gfl.12104.

Turner F.J.; 1968: *Metamorphic petrology mineralogical and field aspects, 1st ed*. McGraw-Hill, New York, NY, USA, 403 pp.

Turner S. and Costa F.; 2007: *Measuring timescales of magmatic evolution*. Elements, 3, 267-272.

U.S. Government Printing Office; 1976: *Standard Atmosphere*. Washington, D.C., USA, 243 pp.

Verdoya M., Pasquale V., Chiozzi P. and Kukkonen I.T.; 1998: *Radiogenic heat production in the Variscan crust: new determinations and distribution models in Corsica (northwestern Mediterranean)*. Tectonophys., 291, 63-75.

Verdoya M., Chiozzi P., Gola G. and El Jbeily E.; 2019: *Conductive heat flow pattern of the central-northern Apennines, Italy*. Int. J. Terr. Heat Flow Appl. Geotherm., 2, 37-45.

Verdoya M., Chiozzi P. and Gola G.; 2021: *Unravelling the terrestrial heat flow of a young orogen: The example of the northern Apennines*. Geotherm., 90, 101993-102006, doi: 10.1016/j.geothermics.2020.101993.

Wagner W. and Kretzschmar H.-J.; 2008: *International steam tables - Properties of water and steam based on the industrial formulation IAPWS-IF97, 2nd ed*. Springer-Verlag, Berlin Heidelberg, Germany, 410 pp., doi: 10.1007/978-3-540-74234-0.

Wang H. and Currie C.A.; 2015: *Magmatic expressions of continental lithosphere removal.* J. Geophys. Res.: Solid Earth, 120, 7239-7260.

Weaver B. and Tarney J.; 1984: *Empirical approach to estimating the composition of the continental crust*. Nature, 310, 575-577, doi: 10.1038/310575a0.

Wen B., Chini G.P., Dianati N. and Doering C.R.; 2013: *Computational approaches to aspect-ratio-dependent upper bounds and heat flux in porous medium convection*. Phys. Lett. A, 377, 2931-2938.

Wright A.E.; 1989: *Metamorphic facies*. In: Petrology, Encyclopedia of Earth Science, Springer, Boston, MA, USA, pp. 324-330, doi.org/10.1007/0-387-30845-8_137.

Corresponding author: Gianluca Gola
Institute of Geosciences and Earth Resources, National Research Council of Italy
Via Giuseppe Moruzzi 1, 56124 Pisa, Italy
Phone: +39 050 621 3268; e-mail: g.gola@igg.cnr.it